

SCIENTIFIC REPORTS



OPEN

NAMPT knockdown attenuates atherosclerosis and promotes reverse cholesterol transport in ApoE KO mice with high-fat-induced insulin resistance

Received: 05 October 2015

Accepted: 21 April 2016

Published: 27 May 2016

Shengbing Li^{1,*}, Cong Wang^{1,*}, Ke Li^{1,*}, Ling Li², Mingyuan Tian¹, Jing Xie¹, Mengliu Yang¹, Yanjun Jia¹, Junying He¹, Lin Gao³, Guenther Boden⁴, Hua Liu⁵ & Gangyi Yang¹

NAMPT has been suggested association with atherosclerosis and insulin resistance. However, the impact of NAMPT on atherosclerosis remained unknown. Therefore, the objective of this study was to use a NAMPT loss-of-function approach to investigate the effect of NAMPT on atherosclerosis in hypercholesterolemic mice. We demonstrated that a specific NAMPT knockdown increased plasma HDL-C levels, reduced the plaque area of the total aorta en face and the cross-sectional aortic sinus, decreased macrophage number and apoptosis, and promoted RCT in HFD-fed ApoE KO mice. These changes were accompanied by increased PPAR α , LXR α , ABCA1 and ABCG1 expressions in the liver. NAMPT knockdown also facilitated cholesterol efflux in RAW264.7 cells. We further investigated the effect of NAMPT knockdown on the PPAR α -LXR α pathway of cholesterol metabolism with MK886 (a selective inhibitor of PPAR α) in RAW264.7 macrophages. MK886 abolished the ability of NAMPT knockdown to decrease intracellular cholesterol levels to enhance the rate of ³H-cholesterol efflux and to increase ABCA1/G1 and LXR α expressions in RAW264.7 macrophages. Our observations demonstrate that NAMPT knockdown exerted antiatherogenic effects by promoting cholesterol efflux and macrophage RCT through the PPAR α -LXR α -ABCA1/G1 pathway *in vitro* and *in vivo*.

Nicotinamide phosphoribosyltransferase (NAMPT) was originally identified as pre-B cell colony enhancing factor (PBEF)¹. Later, NAMPT was thought to be secreted predominantly by visceral adipose tissue and to improve insulin sensitivity *in vivo*^{2,3}. More recently, NAMPT has been identified as an enzyme involved in NAD biosynthesis⁴ and postulated to play an important role in the regulation of cellular metabolism and insulin secretion^{5,6}. However, clinical studies have provided controversial results concerning the role of NAMPT in obesity and glucose metabolism^{7–11}. Therefore, it is currently unclear if NAMPT is involved in the development of insulin resistance (IR) or atherosclerosis.

It has also been reported that NAMPT expression is increased in unstable coronary artery plaques in humans. Immunohistochemical analysis of unstable plaques revealed higher NAMPT concentration compared to stable plaques². It has also been shown that NAMPT induced the release of inflammatory cytokines, cholesterol accumulation and the formation of macrophage foam cells^{12–14}. In addition, we and others have reported that NAMPT is involved in the regulation of serum cholesterol metabolism³. These studies suggest an association between NAMPT and atherosclerosis. Unfortunately, a homozygous knockout model for the NAMPT gene was

¹Department of Endocrinology, the Second Affiliated Hospital, Chongqing Medical University, 400010 Chongqing, China. ²The Key Laboratory of Laboratory Medical Diagnostics in the Ministry of Education and Department of Clinical Biochemistry, College of Laboratory Medicine, Chongqing Medical University, 400010 Chongqing, China. ³Department of Endocrinology, the Affiliated Hospital, Zunyi Medical College, 563003 Guizhou, China. ⁴The Division of Endocrinology/Diabetes/Metabolism and the Clinical Research Center, Temple University School of Medicine, Philadelphia, Pennsylvania, USA. ⁵Department of Pediatrics, University of Mississippi Medical Center, 2500 North State Street, Jackson, Mississippi, MS 39216-4505, USA. *These authors contributed equally to this work. Correspondence and requests for materials should be addressed to G.Y. (email: gangyiyang@163.com)

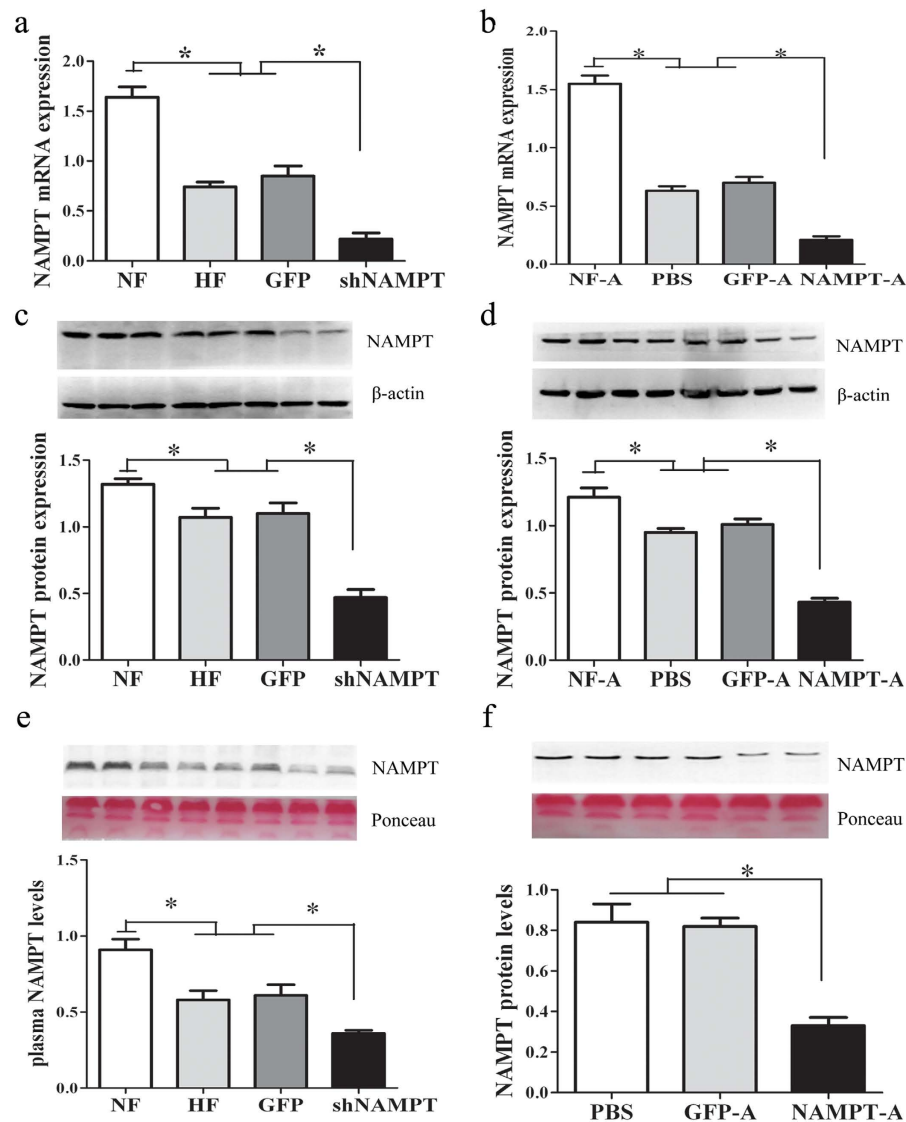


Figure 1. Treatment with Ad-*sh*NAMPT decreases liver expression and plasma levels of NAMPT.

(a) Hepatic NAMPT mRNA expression in C57BL/6J mice. (b) Hepatic NAMPT mRNA expression in ApoE KO mice. (c) Hepatic NAMPT protein expression in C57BL/6J mice. (d) Hepatic NAMPT protein expression in ApoE KO mice. (e) Plasma NAMPT levels in C57BL/6J mice. (f) Plasma NAMPT levels in ApoE KO mice. Data are means \pm SE. $n \geq 8$ per group. * $P < 0.01$. NF, standard chow diet-fed C57BL/6J mice; HF, high fat diet-fed C57BL/6J mice; GFP, high fat diet-fed C57BL/6J mice treated with Ad-GFP; *sh* NAMPT, high fat diet-fed C57BL/6J mice treated with Ad-*sh* NAMPT; NF-A, standard chow diet-fed ApoE KO mice; PBS, high fat diet-fed ApoE KO mice treated with PBS; GFP-A, high fat diet-fed ApoE KO mice treated with Ad-GFP; NAMPT-A, high fat diet-fed ApoE KO mice treated with Ad-*sh* NAMPT.

incompatible with life, with death occurring in the initial phase of embryogenesis. The lack of knock-out mouse of NAMPT has made it difficult to systematically investigate the role of NAMPT in the development of IR and atherosclerosis.

In the present study, we have taken advantage of the relative tissue specificity of adenovirus for liver and the genetic specificity of shRNA-mediated RNAi to create a relative liver-specific deficiency of NAMPT expression, and examined the role of NAMPT in IR and atherosclerosis by using it to inhibit NAMPT expression in mice.

Results

Expressions of NAMPT mRNA and protein in liver and plasma. A previously validated shRNA sequence against NAMPT was engineered into an adenovirus vector (Ad-*sh*NAMPT) and tested for relative silencing efficiency compared with Ad-GFP. In HFD-fed C57BL/6J mice, the expressions of NAMPT mRNA and protein were reduced by 55% and 25% respectively in the liver compared with normal-chow controls (Fig. 1a,c), whereas Ad-*sh*NAMPT treatment, but not Ad-GFP, achieved a ~71% and ~57% reduction in NAMPT mRNA and protein expressions respectively in the liver (both $P < 0.01$; Fig. 1a,c). When compared with the HF and GFP

Treatment	PBS	GFP-A	NAMPT-A
Body weight (g)	33.10 ± 0.95	34.56 ± 0.84	33.65 ± 1.07
FBG (mmol/L)	7.46 ± 0.33	7.25 ± 0.28	7.43 ± 0.27
FIns (mU/L)	82.99 ± 2.33	83.15 ± 2.81	85.71 ± 2.98
TC (mmol/L)	15.03 ± 0.74	15.35 ± 0.65	16.01 ± 0.61
TG (mmol/L)	1.88 ± 0.04	1.92 ± 0.07	1.96 ± 0.05
FFA (mmol/L)	2.44 ± 0.06	2.54 ± 0.07	2.49 ± 0.04
HDL-C (mmol/L)	3.34 ± 0.08	3.38 ± 0.12	4.09 ± 0.09***
LDL-C (mmol/L)	7.63 ± 0.30	7.90 ± 0.35	7.60 ± 0.22
Hepatic TG (mg/gr tissue)	35.09 ± 1.77	34.59 ± 2.28	33.87 ± 1.99
Hepatic TC (mg/gr tissue)	5.57 ± 0.39	5.38 ± 0.38	4.30 ± 0.31**

Table 1. Metabolic parameter for HFD-fed ApoE KO mice. TC, Total cholesterol; TG, Triglyceride; FFA, Free fatty acids; HDL-C, high density lipoprotein cholesterol; LDL-C, low density lipoprotein cholesterol. PBS, HFD-fed ApoE KO mice treated with PBS; GFP-A, HFD-fed ApoE KO mice treated with Ad-GFP; NAMPT-A, HFD-fed ApoE KO mice treated with Ad-*sh*NAMPT. Data are means ± SE (n = 10 per group). **P* < 0.05, ***P* < 0.01 vs. PBS group; #*P* < 0.05, ##*P* < 0.01 vs. GFP-A group.

groups, Ad-*sh*NAMPT treatment also led to a 52% reduction in plasma NAMPT levels (*P* < 0.01, Fig. 1e), demonstrating the efficacy of Ad-*sh*NAMPT *in vivo*. Similarly, in HFD-fed ApoE KO mice (PBS group), the mRNA and protein expressions of NAMPT in the liver were significantly decreased compared with those of SCD-fed ApoE KO mice (NF-A group) (both *P* < 0.01, Fig. 1b,d). Importantly, the mRNA and protein expressions of NAMPT in the liver and NAMPT plasma levels were further decreased by Ad-*sh* NAMPT treatment (all *P* < 0.01, Fig. 1b,d,f).

NAMPT knockdown fails to affect HFD-induced insulin resistance. We next assessed the effects of NAMPT knockdown on metabolic parameters. Values of body weight and fasting blood glucose (FBG), lipid and fasting insulin (FIns) levels were significantly higher in HFD-fed C57BL/6J mice. HDL-C and FIns in Ad-*sh* NAMPT treated plus HFD-fed mice were significantly higher than those of their littermates fed HFD alone (Supplemental Table S1). To assess the effects of NAMPT knockdown on insulin sensitivity, euglycemic- hyperinsulinemic clamps (EHCs) were performed. As shown in Supplemental Table S2, during the clamps, TG, TC, FFA and HDL-C levels were suppressed by hyperinsulinemia in four groups, but HDL-C remained higher in the Ad-*sh* NAMPT group than in the other three groups (*P* < 0.01). The glucose infusion rate (GIR) required was 50% lower in HFD-fed mice compared with SCD-fed controls. Ad-*sh* NAMPT treatment had no effect on the GIR and glucose disposal rate (GRd). In addition, the ability of insulin to suppress hepatic glucose production (HGP) was unchanged in the HFD-fed plus Ad-*sh*NAMPT treated mice compared with HFD-fed mice alone (Supplemental Table S2).

Effect of NAMPT knockdown on metabolic parameters in HFD-fed ApoE KO mice. As shown in Table 1 and Supplemental Fig. S1, Ad-*sh*NAMPT treatment in HFD-fed ApoE KO mice significantly increased HDL-C and apoA-I levels compared with PBS and Ad-GFP treatment. However, there were no differences in the other parameters. In addition, Ad-*sh*NAMPT treatment decreased hepatic TC content to 76% of that in ApoE KO mice fed HFD (*P* < 0.05), whereas hepatic TG content remained unchanged (Table 1).

NAMPT knockdown markedly inhibits the formation of atherosclerotic lesions. As shown in Supplemental Fig. S2, immunohistochemistry found that the expression of NAMPT in the atherosclerotic plaques of Ad-*sh*NAMPT mice was significantly decreased compared with that of Ad-GFP or PBS mice (*P* < 0.01), suggesting that NAMPT signaling was inhibited. To investigate the effects of NAMPT knockdown on the formation of atherosclerotic plaques, atherosclerotic lesions in the aorta were analyzed by en face analysis of the spread total aorta and analysis of cross sections of the aortic sinus. The en face plaque area of the total aorta stained with oil red O was reduced by 67% in HFD-fed and Ad-*sh*NAMPT treated ApoE KO mice compared with HFD-fed ApoE KO mice alone (Fig. 2a). In addition, the cross-sectional plaque area of the aortic sinus stained with H&E was reduced by 54% in Ad- HFD-fed and *sh*NAMPT-treated ApoE KO mice compared with HFD-fed mice alone (Fig. 2b). In Ad-*sh*NAMPT treated mice, oil red O staining also revealed a ~50% decrease in lipid deposition of aortic sinus lesions, whereas picosirius red staining showed a 2-fold increase in collagen content in plaque areas (Fig. 2c,d). To investigate whether NAMPT knockdown also affects the plaque phenotype, we examined two key parameters as surrogate markers for lesion vulnerability. We found that plaques from aortic root of Ad-*sh*NAMPT-treated ApoE KO mice exhibited fewer CD68⁺ macrophages as compared with control littermates (Fig. 3a). In agreement with that, the presence of α-SMA positive cells was increased in Ad-*sh*NAMPT-treated mice (Fig. 3b) as was the accumulation of collagen. Meanwhile, immunofluorescent costaining with CD68 and TUNEL displayed a decrease in the percentage of CD68/TUNEL positive cells in the atherosclerotic plaque of Ad-*sh*NAMPT mice (Fig. 3c).

Effect of NAMPT knockdown on macrophage cholesterol efflux. We loaded macrophages with ³H cholesterol plus HDL and determined HDL-mediated efflux of cholesterol by measuring the appearance of

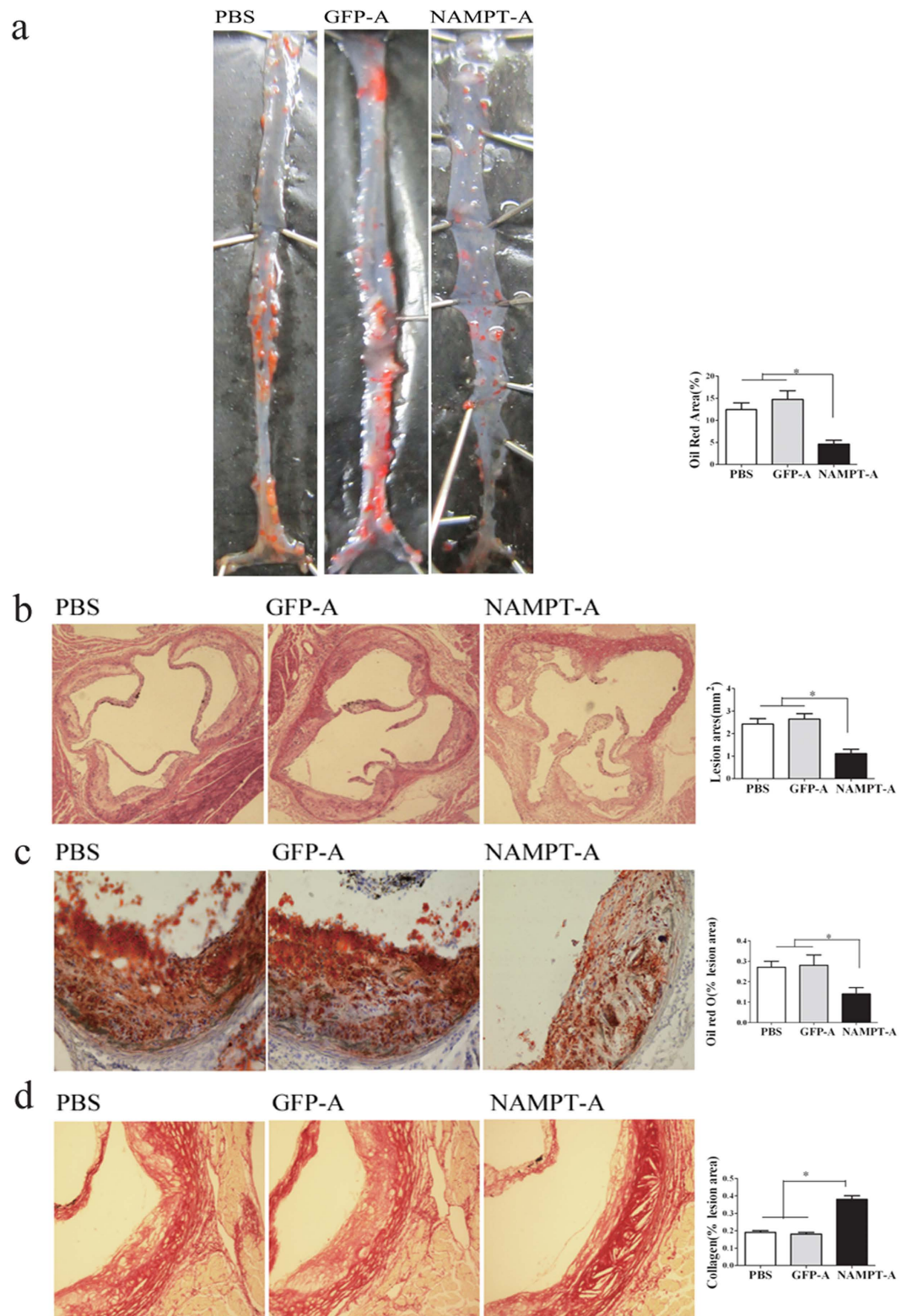


Figure 2. Ad-*sh*NAMPT administration attenuates atherosclerotic lesion in the entire aorta and aortic roots of ApoE KO mice. (a) Representative Oil Red O stained *en face* aortae from ApoE KO mice (left) and quantitative assessment of plaque surface area in the entire aorta (right). (b) Representative H&E stained aortic root cross sections from ApoE KO mice (left) and quantitative assessment of plaque area in the aortic root (right). (c) Representative Oil Red O stained aortic root cross sections for the assessing of lipid deposition in ApoE KO mice (left) and quantitative assessment of the plaque area (right). (d) Representative picrosirius red stained aortic root cross sections for the assessing of collagen contents in ApoE KO mice (left) and quantitative assessment of the plaque area (right). Data are the mean \pm SE. $n = 10$ per group. Original magnification: $\times 40$ (B), $*P < 0.01$.

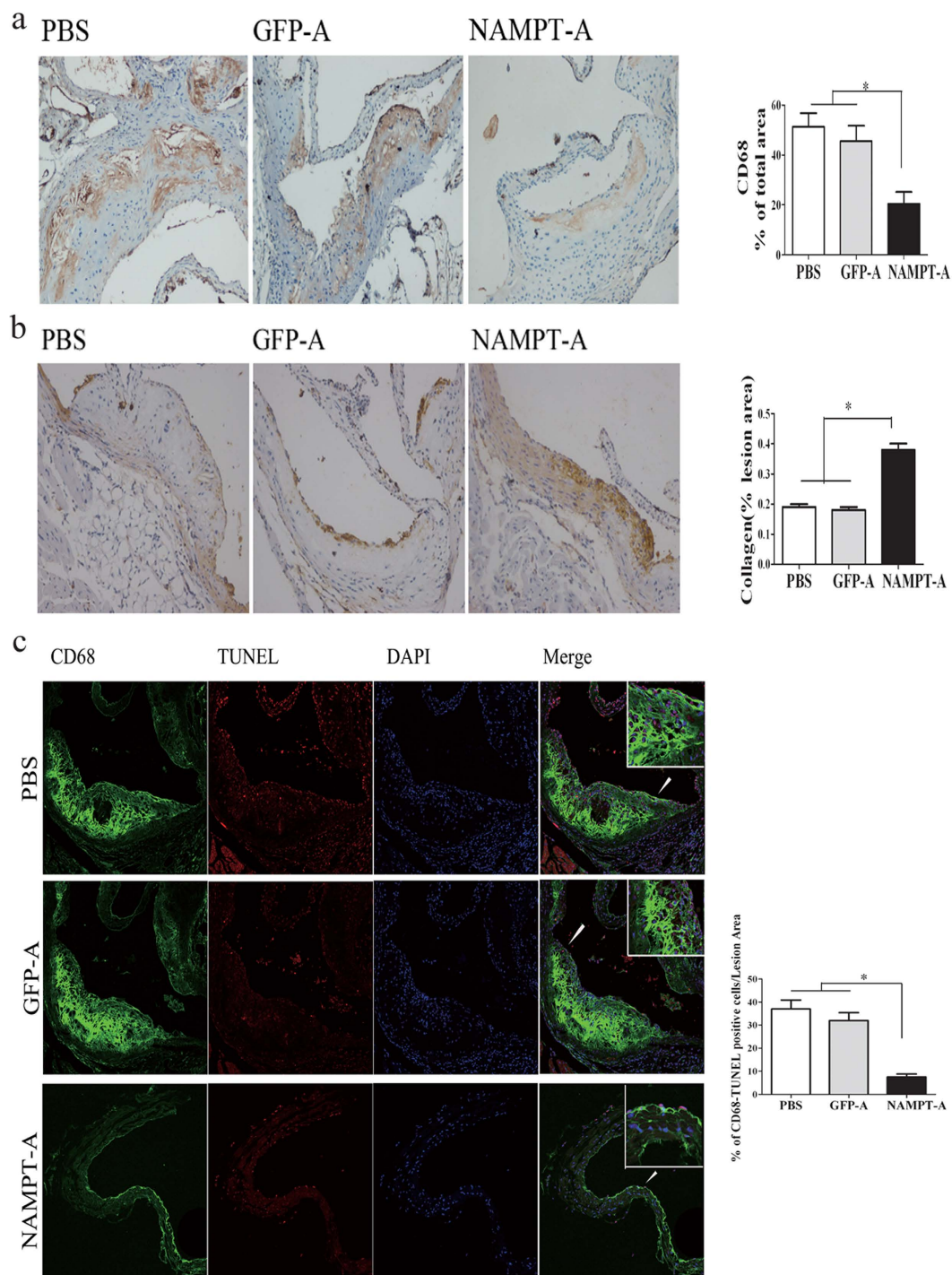


Figure 3. Ad-*sh*NAMPT administration improves a more stable phenotype of atherosclerotic lesions. (a) Representative photomicrographs of aortic roots from ApoE KO mice stained with an antibody against CD68 for macrophages (left) and quantitative assessment of the plaque area (right). (b) Representative immunohistochemical staining of aortic roots from ApoE KO mice for α -SMA (left) and quantitative assessment of the plaque area (right). (c) Apoptotic cells in the lesion area were detected by TUNEL staining, and macrophages by CD68 staining. Representative images ($\times 20$ magnification) are shown left and quantitative data are shown right. Data are the mean \pm S.E. Magnification $\times 200$, $*P < 0.01$.

cholesterol in the medium. NAMPT treatment decreased ^3H cholesterol release in a concentration-dependent fashion (Supplemental Fig. S3). To determine if NAMPT deficiency influences macrophage cholesterol efflux, we conducted *in vitro* assays testing effects of Ad-*sh*NAMPT treatment on cholesterol efflux from ^3H -cholesterol-loaded RAW cells to lipoprotein acceptors. In Ad-*sh*NAMPT -treated cells, both NAMPT

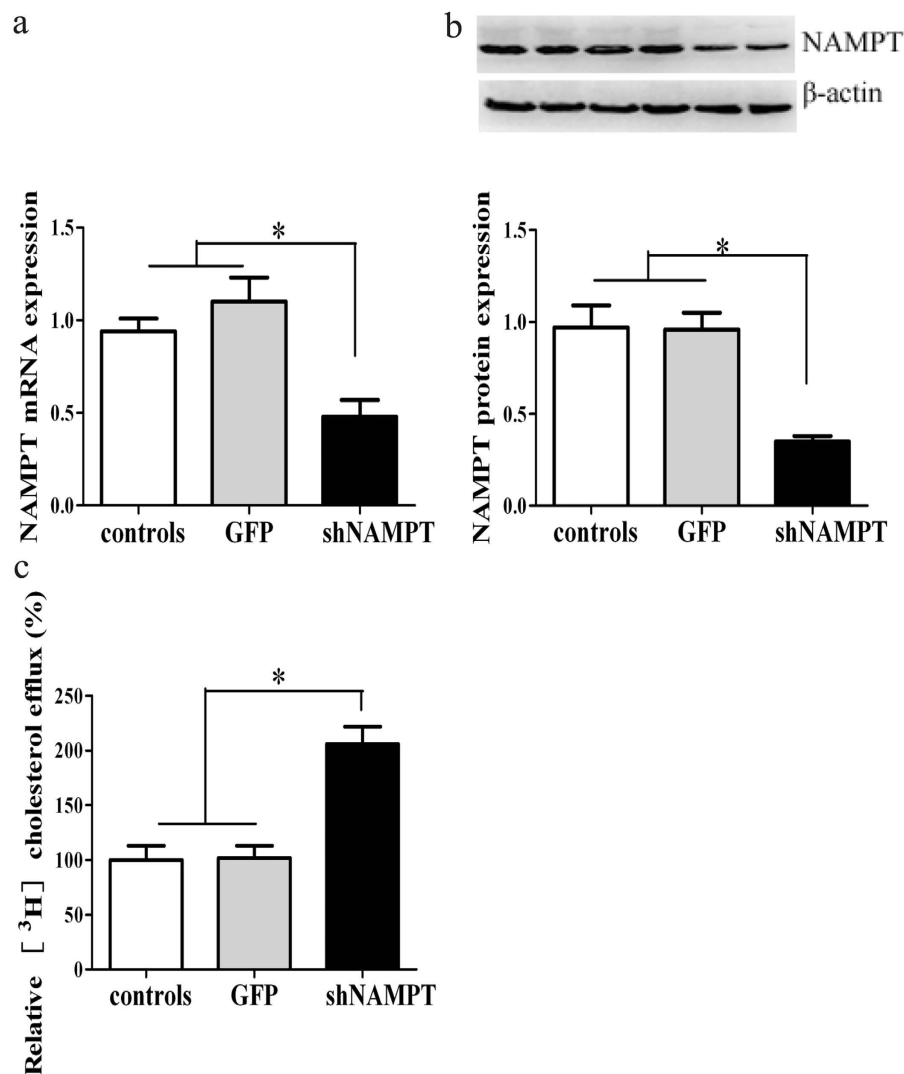


Figure 4. NAMPT knockdown promotes the HDL-mediated cholesterol efflux in RAW cells. (a) NAMPT mRNA expression in RAW cells. (b) NAMPT protein expression in RAW cells. (c) The HDL-mediated cholesterol efflux in RAW cells. The efflux of untreated cells represents is expressed as 100%. The data represent mean \pm SE in three independent experiments. * $P < 0.01$. Controls, RAW264.7 cells; GFP, RAW cells treated with Ad-GFP; *sh*NAMPT, RAW cells treated with Ad-*sh*NAMPT.

mRNA and protein expressions were significantly decreased (Fig. 4a,b). Ad-*sh*NAMPT treatment promoted the HDL-mediated efflux of ³H-cholesterol from labeled RAW cells by 106%, suggesting that NAMPT deficiency is able to activate the cholesterol efflux that exports excess cholesterol from macrophages (Fig. 4c).

NAMPT knockdown increases HDL-C and enhances RCT *in vivo*. We next analyzed the lipoprotein profiles in plasma from three groups of mice by FPLC. The results showed that the increased plasma cholesterol in Ad-*sh*NAMPT mice was mainly in the HDL fractions (column fractions 26–31), with no difference in the VLDL and LDL regions (Fig. 5a).

To determine whether Ad-*sh*NAMPT treatment triggers higher HDL-C levels in response to upregulation of cholesterol transport from peripheral cells to the liver for further excretion into bile, we performed an *in vivo* RCT assay that traces ³H-cholesterol derived from macrophages loaded with cholesterol *ex vivo*. After intraperitoneal injection of ³H-cholesterol-labeled macrophages, plasma ³H-cholesterol levels at 6, 24 and 48 h after injection were significantly higher in Ad-*sh*NAMPT mice compared with PBS- and Ad-GFP-treated mice (Fig. 5b). Ad-*sh*NAMPT mice showed a 44% increase in the delivery of macrophage-derived ³H-tracer to the liver and a 35% increase in ³H-sterols excreted into feces (Fig. 5c,d). Therefore, NAMPT inhibition not only increases circulating HDL-C, but also enhances the RCT pathway by which excess cholesterol is effluxed from peripheral tissues.

Effects of NAMPT knockdown on gene expressions related to cholesterol metabolism in the liver. Next, we found that the PPAR α , LXR α , ABCA1 and ABCG1 mRNA and protein contents in the liver were markedly increased in Ad-*sh*NAMPT treated mice compared with control mice (Fig. 6a,b).

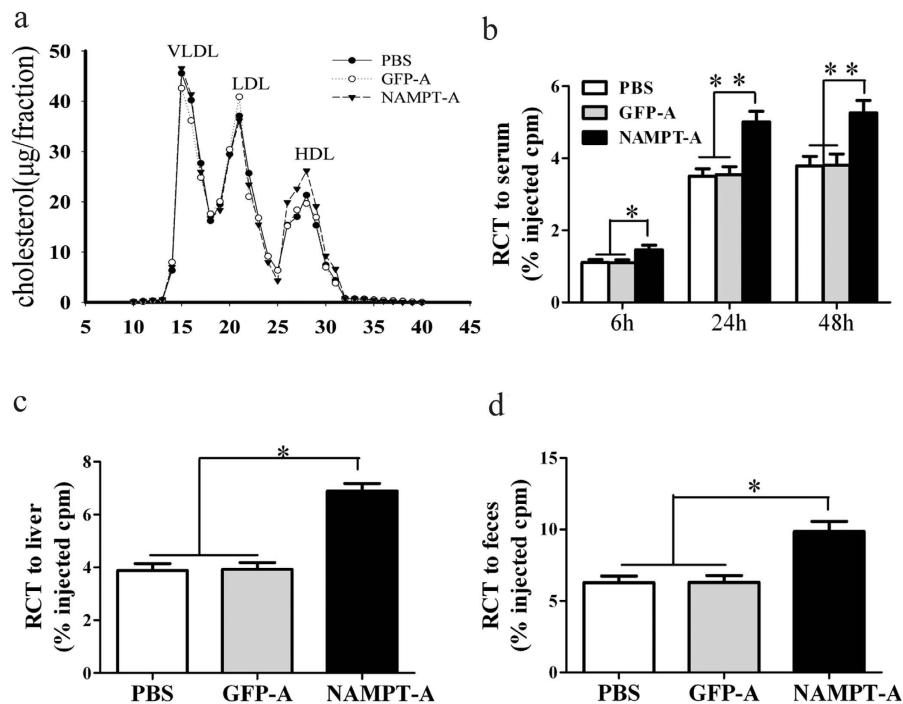


Figure 5. NAMPT deficiency increases plasma HDL-C concentration and promotes RCT in HFD-fed ApoE KO mice. (a) FPLC analysis of plasma lipoprotein distribution from ApoE KO mice. Each profile represents a separation of a plasma pool from 8 mice of each group. (b) Time course of ^3H -cholesterol distribution in plasma. (c) Hepatic ^3H -cholesterol tracer levels after 48 hours. (d) Fecal ^3H -cholesterol tracer levels. Feces were collected continuously from 0 to 48 hours after injection. Data are expressed as the percentage of the ^3H -cholesterol tracer relative to total cpm tracer injected \pm SE. * $P < 0.05$, ** $P < 0.01$. RCT, macrophage reverse cholesterol transport; HDL-C, High-density lipoprotein cholesterol; other abbreviations as in Fig. 1.

NAMPT knockdown-induced reduction in cholesterol levels and the expression of PPAR α is blocked *in vitro* by MK886. Because of the well-documented stimulatory role of PPAR- α activators on hepatic HDL production and ABCA1-mediated cholesterol efflux from macrophages¹⁵, we investigated the effects of Ad-*sh*NAMPT on cholesterol metabolism and the PPAR α /LXR α /ABCA1/ABCG1 pathway in RAW cells. Ad-*sh*NAMPT treatment in RAW cells led to an 81% and a 68% decrease respectively in the expression of NAMPT mRNA and protein (Fig. 7a). We further studied the effects of NAMPT knockdown on cholesterol metabolism and the expression of genes involved in cholesterol efflux and the RCT pathway in these cells. In RAW cells, Ad-*sh*NAMPT led to a 33% decrease in total cholesterol levels (Fig. 7b). However, this effect was negated by the coadministration of MK886, a selective inhibitor of PPAR α (Fig. 7b). Ad-*sh*NAMPT treated cells resulted in a 121% increase of ^3H -cholesterol efflux to HDL compared to that of untreated cells, whereas, this effect was inhibited by MK886 (Fig. 7c). Consistent with the changes observed for cholesterol levels, ABCA1, ABCG1, PPAR α and LXR α mRNA and protein were significantly increased in Ad-*sh*NAMPT treated cells (Fig. 7d,e). Importantly, these changes were negated by MK886 treatment (Fig. 7d,e). These findings suggest that the effect of NAMPT on cholesterol metabolism may be mediated via the PPAR α /LXR α /ABCA1/ABCG1 signaling.

Discussion

The absence of NAMPT knock-out models have severely hindered the study of NAMPT's function. To better understand the role of NAMPT deficiency in IR and atherosclerosis, we have developed an adenovirus-mediated RNA interference technique to knock down NAMPT expression *in vivo*. In the present study, we have taken advantage of the relative tissue specificity of adenovirus for liver to create a relative liver-specific deficiency of NAMPT¹⁶. This technique allowed us to investigate the role of NAMPT deficiency without the lifelong loss of function¹⁶. Although systemic administration of adenoviral vectors can cause the inflammatory immune response and cytotoxicity, numerous studies have demonstrated that third-generation adenoviral vectors, as used in this study, are superior to first- and second-generation adenoviral vectors in terms of mediating long-term transgene expression with negligible inflammatory immune response and hepatotoxicity^{17,18}. In support of this notion, we previously reported that our adenoviral vectors failed to increase inflammatory cytokine expressions and inflammation revealed by hematoxylin and eosin histology in the liver¹⁹.

The adenovirus-mediated RNAi resulted in high silencing efficiency and long lasting effects (up to 4 weeks with 2 injections)²⁰. This allowed us to evaluate the metabolic and arteriosclerotic impact of hepatic NAMPT knockdown in an IR animal model. Unexpectedly, HFD-fed mice with reduced hepatic NAMPT content showed no alterations in any of the tested metabolic parameters, except for elevated HDL-C and slightly decreased LDL-C levels which were not statistically significant. We then performed EHCs for an in-depth analysis of the effects of

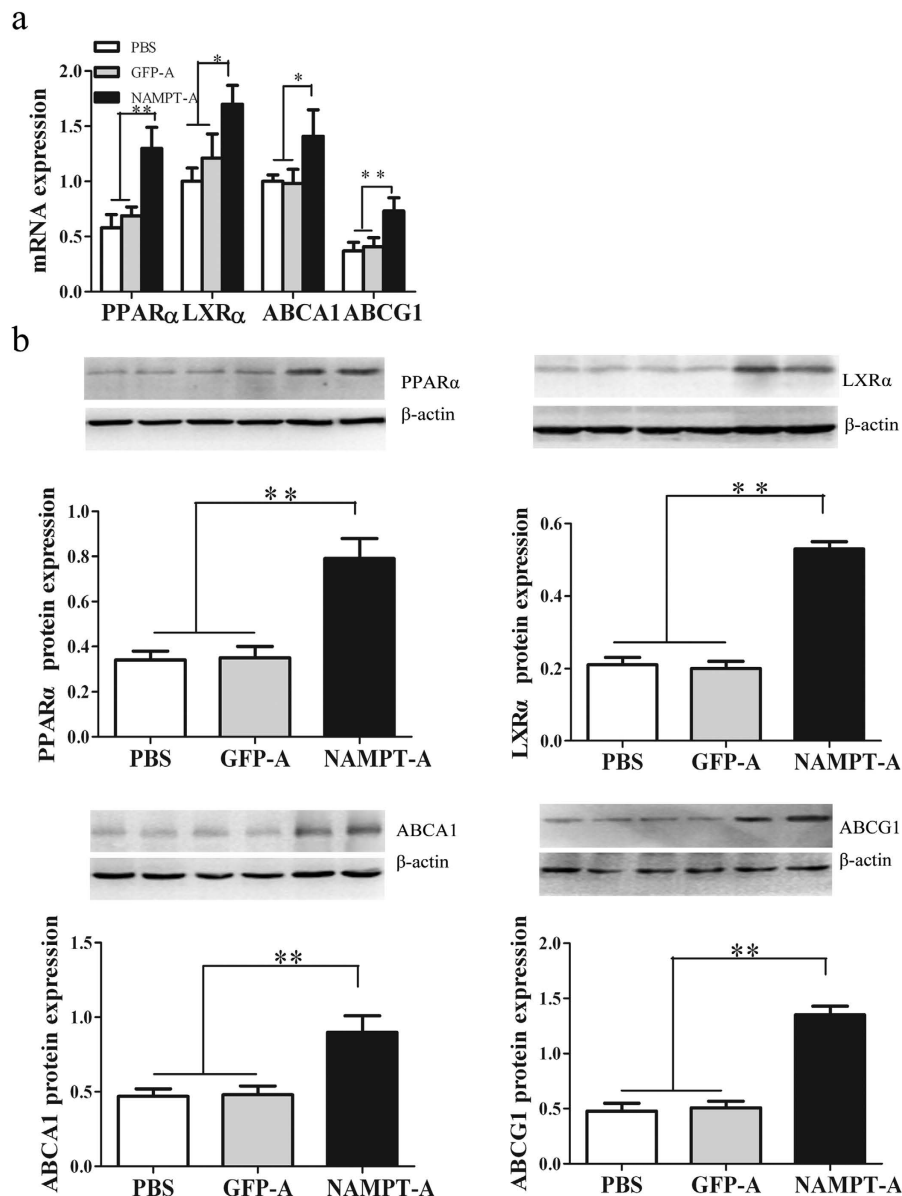


Figure 6. The effects of NAMPT deficiency on mRNA and protein expression of hepatic genes involved in cholesterol metabolism in HFD-fed ApoE KO mice. (a) Analysis of hepatic gene expression by real-time quantitative PCR. (b) Analysis of hepatic gene expression by Western blots. Data are means \pm SE. $n = 5$ per group. * $P < 0.05$, ** $P < 0.01$. PPAR α , Peroxisome proliferator-activated receptors- α ; LXR α , Liver X receptor- α ; ABCA1, ATP binding cassette transporters A-1; ABCG1, ATP binding cassette transporters G-1.

NAMPT knockdown on insulin sensitivity. Surprisingly, these clamp studies showed that GIR, HGP, and GRD were unchanged in HFD-fed mice treated with Ad-*sh*NAMPT suggesting that NAMPT knockdown did not impact insulin sensitivity *in vivo*.

However, we noted a trend of elevated HDL-C and apoA-I levels in HFD-fed mice with NAMPT knockdown. This led us to investigate whether NAMPT knockdown affected cholesterol metabolism and the development of atherosclerosis. For this purpose, we treated HFD-fed ApoE KO mice with Ad-*sh*NAMPT and examined metabolic parameters and atherosclerotic lesions. We observed that plasma HDL-C levels in HFD-fed ApoE KO mice treated with Ad-*sh*NAMPT were significantly increased and hepatic TC contents were decreased compared to littermates fed HFD alone. Analysis of lipoproteins showed an increase in cholesterol content in the HDL fractions of Ad-*sh*NAMPT-treated mice, suggesting that NAMPT may be important for cholesterol metabolism. Currently, it is widely accepted that even subtle changes in HDL cholesterol may have profound effects on the development of atherosclerosis. Therefore, we investigated the effects of *in vivo* NAMPT on atherosclerotic lesions in the aorta. We found that NAMPT deficiency attenuated atherosclerotic lesions in the entire aorta and the aortic sinus and reduced lipid accumulation in aortic sinus lesions. Although lesion size accurately reflects atherosclerosis progression, plaque phenotype is a more important predictor of plaque disruption and acute clinical events

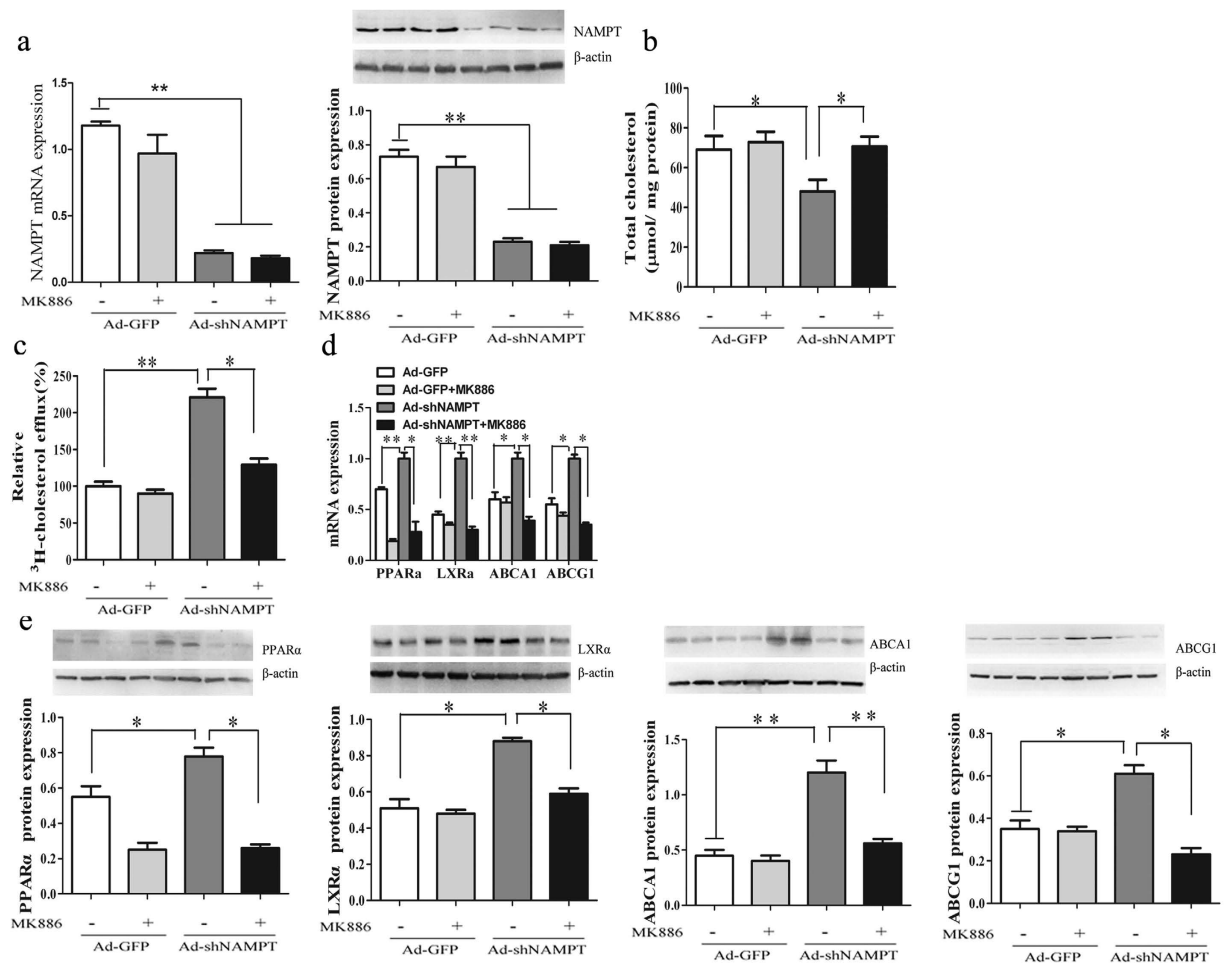


Figure 7. NAMPT deficiency stimulates the expression of LXR α , ABCA1 and ABCG1 and decreased cholesterol levels via PPAR α -dependent mechanisms. RAW cells were transduced with Ad-GFP or Ad-shNAMPT in the presence or absence of MK886. (a) NAMPT mRNA (left) and protein expression (right). (b) Cellular cholesterol levels. (c) The HDL-mediated cholesterol efflux. (d) PPAR α , LXR α , ABCA1 and ABCG1 mRNA expression. (e) PPAR α , LXR α , ABCA1 and ABCG1 protein expression. Data represent the mean \pm SE from three independent experiments. * $P < 0.05$, ** $P < 0.01$. MK886, a selective inhibitor of PPAR α .

in humans²¹. Therefore, we evaluated several key parameters as surrogate markers for lesion vulnerability. Our findings indicate that NAMPT knockdown in ApoE KO mice decreased lipid content, CD68⁺ macrophages, macrophage apoptosis, and increased α -SMA positive cells and the accumulation of collagen in atherosclerotic plaque. These data indicate that NAMPT knockdown reduced atherosclerotic plaque macrophage infiltration and lesion burden by modifying plaque composition, which reflected a stable atherosclerotic plaque phenotype. Here, NAMPT knockdown seemed to exert contradictory effects in these experiments, protecting against atherosclerosis without changing insulin sensitivity. Therefore, we speculated that the reduction of hepatic NAMPT expression in both HFD-fed C57BL/6J and ApoE KO mice might be a compensatory down-regulation to counteract the metabolic stress imposed by obesity or abnormal cholesterol metabolism. This down-regulation may play a role in preventing atherosclerotic progression. We also considered the possibility that the antiatherogenic effects of NAMPT knockdown could have been due to other factors, such as macrophage recruitment, cholesterol efflux to HDL and changes in RCT. Consequently, we investigated the effect of NAMPT knockdown on these factors.

The RAW 264.7 cell line is a model widely used to study macrophage regulation of cholesterol efflux. We found that in cultured RAW264.7 cells, HDL-mediated ³H-cholesterol efflux was increased by NAMPT knockdown, suggesting that NAMPT knockdown led to an increase in the ability of cells to efflux intracellular cholesterol to HDL and therefore to promote the initial step of macrophage RCT. However, this observation contradicted previous findings by Dahl T *et al.*²², who reported that a reduction in cholesterol efflux in ox-LDL-exposed macrophages was induced by FK866, a pharmacological inhibitor which mediated inhibition of intracellular NAMPT. The reason for this difference is not clear but may be related to: 1) differences in study protocol, conditions and methods. For example, their studies were performed with ³H-cholesterol and ox-LDL treated THP-1 cells, whereas we used ³H-cholesterol-treated RAW264.7 cells; 2) the different pharmacological and molecular inhibition of NAMPT; 3) the inability of FK866 to block NAMPT from triggering the IL-6/STAT3 cell survival

pathway²³ and lastly, 4) ox-LDL has been reported to enhance NAMPT expression in THP-1 cells²². Thus, further studies are needed to confirm the role of NAMPT in cholesterol efflux.

As RCT is believed to be a critical mechanism by which HDL-C exerts its protective effects on atherosclerosis, we performed an *in vivo* RCT assay that traces ³H-cholesterol from macrophages, loaded *ex vivo* with cholesterol. Consistent with the *in vitro* cholesterol efflux, results of the RCT showed that higher HDL-C levels in response to NAMPT knockdown increased cholesterol transport from peripheral macrophages to the liver. Therefore, NAMPT inhibition not only increased circulating HDL-C, but also enhanced RCT by which excess cholesterol is effluxed from peripheral tissues, a process that is particularly important in the removal of cholesterol from atherosclerotic lesions. These results also suggest that reduced circulating NAMPT produced from the liver and/or other tissue might be the main explanation for increased cholesterol efflux from the injected RAW cells. As the outcome of numerous studies has shown that the rate of macrophage RCT has a greater influence on the degree of atherosclerosis than the levels of HDL-C²⁴, this increase in RCT could be primarily responsible for the positive effects of NAMPT knockdown on atherosclerosis. These data establish NAMPT inhibition as an attractive therapeutic target for raising HDL-C, increasing RCT, and reducing atherosclerosis.

It has been shown that PPAR α activation enhances cholesterol efflux and RCT in association with increased expression of ABCA1/ABCG1 in macrophages via the PPAR α -LXR pathway²⁵. Understanding how NAMPT is integrated into this complex genetic network may reveal novel therapeutic targets for antiatherosclerotic treatment. To better understand the impact of NAMPT on gene expression involved in cholesterol efflux and RCT, we measured the expression of ABCA1, ABCG1, PPAR α and LXR α in the liver. The results demonstrated that NAMPT knockdown upregulated mRNA and protein expressions of these genes. Consistent with these observations, Rotllan *et al.*²⁶ reported that the PPAR α agonist fenofibrate promoted macrophage RCT and enhanced cholesterol efflux and ABCA1/G1 expression in primary macrophages. Together, these observations suggest that NAMPT inactivation promotes cholesterol efflux and macrophage RCT via a complex pathway involving ABCA1/G1, PPAR α and LXR α . These results support the concept that promotion of macrophage RCT may be one mechanism by which NAMPT knockdown inhibits the development of atherosclerosis in hypercholesterolemic mice. Moreover, our present data suggested that an important factor in the promotion of overall RCT and cholesterol efflux by NAMPT knockdown was activation of PPAR α . We, therefore, examined whether PPAR α plays a role in the promotion of RCT by NAMPT knockdown by using MK886 (a selective inhibitor of PPAR α) in RAW cells. Noteworthy, MK-886 is also an inhibitor of leukotriene biosynthesis. Prolonged treatment with the 5-lipoxygenase inhibitor MK-886 reduced development of atherosclerosis by inhibiting inflammatory responses in animal model^{27,28}. Therefore, the role of MK886 may be a bilateral regulator for inflammatory responses and atherosclerosis^{29,30}. In addition, MK886 has been shown to be a non-competitive inhibitor of PPAR α activity. It inhibits PPAR α activity though its impact on the transcriptional levels of PPAR α promote-driven reporter^{31–34}. In the current study, we found that MK886 negated NAMPT knockdown-induced ABCA1/G1 and LXR α expressions in these cells. Moreover, MK886 treatment negated the effect of NAMPT knockdown on intracellular cholesterol levels and the rate of ³H-cholesterol efflux. Collectively, our *in vivo* and *ex vivo* findings are consistent with the concept that NAMPT knockdown enhances cholesterol efflux in association with increased expression of ABCA1/G1 in the liver, resulting in promotion of overall RCT via the PPAR α -LXR α pathway.

During the preparation of our paper, Nencioni *et al.* reported that treatment with FK866, a NAMPT inhibitor, reduced neutrophil infiltration and MMP-9 content and increased collagen levels in atherosclerotic plaques in ApoE KO mice³⁵. However, they did not examine effects of NAMPT knockdown on insulin sensitivity, RCT, HDL-mediated ³H-cholesterol efflux or lipoprotein profiles. They also did not evaluate the en face plaque area of the total aorta. Importantly, the mechanism linking NAMPT knockdown to cholesterol metabolism was not delineated in that study.

In summary, this study has provided new information with respect to the role of NAMPT in the development of atherosclerosis. Our findings are schematically presented in Supplemental Fig. S4. Our results indicate that NAMPT knockdown exerts antiatherogenic effects by promoting macrophage RCT through the PPAR α -LXR α pathway, and is consistent with the concept that NAMPT may be a negative regulator of macrophage RCT and the development of atherosclerosis in humans. Therefore, these findings not only reveal a novel function of NAMPT in regulating lipid metabolism and preventing plaque formation, but also underscore as an important therapeutic target for atherosclerosis and cardiovascular diseases.

Methods

Ethics Statement. Animal experiments were performed in adherence with the US National Institutes of Health Guidelines on the use of laboratory animals (NIH Publication No. 85–23, revised 1996) and were approved by the Chongqing Medical University Committee on Animal Care.

Generation of NAMPT knockdown vector. To construct vectors expressing shRNAs against NAMPT, we designed several oligonucleotides and complementary strands to target specifically mouse NAMPT. The sequence 5'-GCGCTTTGCTACAGAAGTTAA -3' was the most effective one and therefore, was selected for subsequent experiments. A recombinant vector Ad-*sh*NAMPT was generated by transfection in 293 cells with the Ad-Easy system. A control recombinant vector Ad-GFP encoding enhanced green fluorescence protein (GFP; Clontech) was used as a control. Large-scale amplification and purification of recombinant adenoviruses were performed using the Virabind Adenovirus Purification Kit (Cell Biolabs Inc., San Diego, CA, USA).

Animal preparation for the *in vivo* experiments. Male C57BL/6J and ApoE KO mice were purchased from The Experimental Animal Center of Beijing University of Medical Sciences (Beijing, China) at 3 weeks of age, and fed either a standard chow diet (SCD, 18% kcal from fat) or a high fat western diet consisting of 42% fat and 0.15% cholesterol (HFD, Research Diets Inc.) for 12 weeks. C57BL/6J mice were injected with Ad-*sh*NAMPT,

Ad-GFP (1×10^9 pfu in 100 μ l of PBS), or sterile saline by tail vein at week 11 of receiving HFD feeding. At week 8 and 10 of HFD feeding, ApoE KO mice were also treated with Ad-*sh*NAMPT, Ad-GFP or sterile saline by tail vein.

Hyperinsulinemic-euglycemic clamps. Thirty eight C57BL/6J mice were randomized into four groups: SCD (NF group, $n = 10$), HFD (HF group, $n = 10$), HFD plus Ad-GFP (GFP group, $n = 8$), HFD plus Ad-*sh*NAMPT (*sh*NAMPT group, $n = 10$). Four days before the clamp studies, animals were anesthetized with ip ketamine (80 mg/kg) and xylazine (16 mg/kg) and catheters were placed into the right internal jugular vein and left carotid artery^{36,37}. Clamp studies were performed in conscious mice as previously described³⁷. In brief, food was removed 8 hours prior to beginning of studies. At $t = -90$ min, a primed, continuous infusion of HPLC-purified [$3\text{-}^3\text{H}$]-glucose (Amersham, Los Angeles, CA, USA; 5 μ Ci bolus, 0.05 μ Ci/min) was initiated and continued for 3.5 hours. At 0 min, a continuous infusion of insulin and a variable infusion of 20% glucose were started. Blood samples (50 μ l) were obtained from the jugular vein catheter at 0, 80, 90, 100 and 120 min for determination of insulin, free fatty acids (FFA) and glucose specific activity. At the end of the clamp, the mice were anesthetized, and tissue samples were freeze-clamped *in situ* with aluminum tongs, pre-cooled in liquid nitrogen and stored at -80°C for subsequent analysis.

Histological analysis. 40 ApoE KO mice were divided into three groups: HFD plus saline mice as diet controls (PBS group, $n = 10$); HFD plus Ad-*sh*NAMPT mice (NAMPT-A group, $n = 10$) and HFD plus Ad-GFP mice (GFP-A group, $n = 10$). Mice were killed with an overdose of isoflurane and exsanguinated by cardiac puncture at the end of two weeks after the second vector injection. Mice were then perfused with 4% paraformaldehyde in PBS. Hearts and descending aortas were excised. Hearts were fixed in paraformaldehyde and then either embedded in paraffin or Optimal Cutting Temperature (OCT). The cross-sections (5 μ m thick) of aortic sinus embedded in paraffin were stained with Hematoxylin and Eosin (H&E) for histological analysis or with Picrosirius Red for collagen analysis as previously described³⁸. For assessing of neutral lipid, the frozen cross-sections (10 μ m thick) of aortic sinus embedded in OCT were stained with Oil Red O, and counterstained with hematoxylin. For analyses of aortic lesions en face, Oil Red O staining of the excised aortas from the arch to the common iliac levels was performed after fixation in phosphate-buffered 10% formaldehyde. Percentages of en face Oil Red O positive areas to total aortic areas were calculated. Quantitative analyses were performed by using the Image Pro-Plus software (Media Cybernetics).

Immunohistochemistry and Immunofluorescence. Paraffin-embedded cross sections of aortic sinus were deparaffinized by immersion in xylene, and were blocked with 5% normal goat serum for 60 min. Sections were incubated with rat anti-mouse NAMPT (1:500; Abcam, Cambridge, UK), CD68 (1:100; Abcam, Cambridge, UK) and alpha smooth muscle actin (α -SMA) (1:500; Abcam, Cambridge, UK) overnight at 4°C . Sections were then washed and incubated with biotinylated secondary antibody (Co Win Biotech, Beijing, China) for 60 min at room temperature. Antigen-antibody complexes were detected with the Avidin-biotin peroxidase for 60 min at room temperature. Bound antibody was visualized with DAB (Co Win Biotech, Beijing, China). Nuclei were counterstained with hematoxylin. Negative control was carried out by substituting the primary antibody with PBS³⁹. For immunofluorescence analyses, the tissue sections were first stained with CD68, followed by TUNEL staining with a situ cell death detection kit (Roche Molecular Biochemicals, Germany) according to the manufacturer's protocol. The nuclei were stained with 40, 6-diamidino-2-phenylindole (DAPI). Images were obtained using a fluorescence microscope (Nikon Eclipse Ti) or digitized microscope (Olympus) and were analyzed by ImagePro plus software (Media Cybernetics)^{40,41}. The quantitation of tissue sections was performed by observers blinded to specimen.

Cell Culture. RAW 264.7 (RAW) macrophages were obtained from the American Type Culture Collection (ATCC, Manassas, VA, USA) and routinely propagated at 37°C in a humidified atmosphere of 5% CO_2 in Dulbecco's modified Eagle's medium (Gibco, Carlsbad, CA) supplemented with 10% fetal bovine serum, 100 μ g/ml penicillin, and 100 μ g/ml streptomycin.

Cholesterol Efflux Assay. RAW cells were grown to 60% confluence in 24-well plates, and then incubated with DMEM containing 1 μ Ci of [$1, 2\text{-}^3\text{H}$] cholesterol per ml for 48 h. RAW cells were washed three times with PBS, and Cellular cholesterol pools were allowed to equilibrate for another 24 h in DMEM containing 0.1% BSA (DMEM-BSA), Ad-GFP or Ad-*sh*NAMPT (10 μ l 1×10^{11} pfu/ml). For dose-dependent experiments, RAW cells were stimulated with recombinant mouse NAMPT (Alexis Biochemicals, Paris, France) in concentrations of (40, 100 and 200 nM) for another 24 h. After intensive washing of cells with PBS-BSA, Efflux studies (24 h) were carried out using 100 μ g of HDL per ml prepared in DMEM-BSA as the cholesterol acceptor. After the efflux period, Medium was collected and centrifuged, and radioactivity was counted by liquid scintillation counting (LSC). The residual radioactivity in the cell fraction was determined after an overnight extraction with hexane-isopropanol (3:2). Percentages of cholesterol efflux to HDL were calculated by dividing the radioactive counts in the efflux medium by the sum of the radioactive counts in the medium and the cell fraction. The values were normalized with untreated control cells expressed as 100%.

Macrophage *in vivo* reverse cholesterol transport (RCT) study. RCT studies were performed as previously described^{42,43}. RAW cells were plated in 6-well plates (2×10^5 cells/well) and 24 hours later were labeled with 5 μ Ci of [$1, 2\text{-}^3\text{H}$] cholesterol and 50 μ g/ml acetylated LDL (AcLDL) in DMEM plus 10% FBS media for 48 h. These foam cells were washed twice, equilibrated in DMEM plus 0.2% BSA for 6 h, spun down, and resuspended in DMEM medium before use. The cholesterol content of cells was markedly elevated, and the majority of cellular cholesterol was esterified, as determined by thin-layer chromatography.

³H-cholesterol-labeled and AcLDL-labeled RAW cells (typically 4.5×10^6 cells containing 6.4×10^6 counts per minute (cpm) in 0.5 ml DMEM) were injected intraperitoneally into HFD-fed ApoE KO Mice treated with PBS, Ad-GFP or Ad-*sh* NAMPT. Prior to injection, an aliquot of cells was counted using LSC to measure baseline radioactivity. Blood was collected at 6, 24, and 48 h, and plasma was used for LSC. Feces were collected continuously from 0–48 h, homogenized in 50% NaOH overnight and counted in an LSC. At 48 hours after injection, mice were killed with an overdose of isoflurane and exsanguinated by cardiac puncture. Mice were perfused with cold PBS, and portions of the liver were removed. Lipids extractions were performed as described⁴⁴, and radioactivity was counted by LSC. RCT to plasma, feces, and liver was calculated as a percentage of total radioactivities injected at baseline.

Studies on the Participation of Peroxisome proliferator-activated receptors- α (PPAR α) in RAW264.7 cells. RAW cells were grown to 60% confluence in 6-well plates, and then incubated with DMEM containing 1 μ Ci of [1, 2-³H] cholesterol per ml for 48 h. Percentages of cholesterol efflux to HDL were determined as mentioned above in RAW cells treatment with Ad-*sh*NAMPT or Ad-GFP in the presence or absence of the selective inhibitor of PPAR α (10 μ M, MK886, Cayman Chemical Company). Total cellular cholesterol was measured using cholesterol assay kits purchased from Applygen Technologies Inc (Beijing, China). Expression of NAMPT, PPAR α , LXR α , ABCA1 and ABCG1 were determined by Real-time RT-PCR and western blot analysis.

Real-time RT-PCR analysis. Total RNA was extracted from tissue (100 mg) and cells using Trizol reagent (Invitrogen, Carlsbad, CA, USA). Real time polymerase chain reaction (qRT-PCR) was performed with a SYBR Green PCR kit (Takara Bio Inc. Otsu, Japan), and a Corbett Rotor Gene 6000 real-time PCR system (Corbett Research, Sydney, Australia) according to the manufacturer's instructions. Gene expressions were analyzed by the comparative Ct method and normalized to β -actin. Forward and reverse primers are listed in Supplemental Table S3.

Western blot analyses. Tissues were homogenized. For the *in vitro* experiments, cell lysates and medium were collected 48 h after transfection. Protein concentration was measured with a BCA protein quantification kit (Pierce Biotechnology). Plasma samples (50 μ l) were diluted 1:10 in PBS, reduced by adding Nupage sample reducing agent (Invitrogen), and heat denatured. Three microliters of the 1:10 diluted samples were loaded on a 10% Novex Bis-Tris gel (Invitrogen). Total protein in plasma was assessed by staining the blot with Ponceau S. Cell lysates or tissue extracts (70 μ g) were separated by SDS-polyacrylamide gel electrophoresis and transferred to PVDF membranes. Immunoblots were then blocked in TBS containing 0.1% Tween-20 and 5% skimmed milk overnight at 4 °C, and then incubated with primary antibodies including anti-NAMPT, anti- ABCA1, anti-ABCG1(abcam, 1:1000 dilution), anti-PPAR α , anti-LXR α (Santa,1:500 dilution)and β -actin (Research Diagnostics) for 24 h at 4 °C. For detection of NAMPT protein in blood, the blot was stained with Ponceau S, and the region covering the 66-kDa protein was cut from the rest as a control⁴⁵. Following 3 washes in TBST, blots were incubated with HRP-conjugated secondary antibody for 1 h. After 2 washes in TBST, the blots were scanned using the Enhanced chemiluminescence (ECL) detection system (Viagene, USA) and quantification of antigen-antibody complexes was performed using Quantity One analysis software (Bio-Rad).

Analytical procedures. Radioactivity [³-³H] glucose, [1-³H]-cholesterol and [1-³H]-sterols were measured by LSC. Plasma FFA was determined spectrophotometrically using an acyl-CoA oxidase-based colorimetric kit (Wako Pure Chemical Industries, Osaka, Japan). Insulin was measured using a commercial insulin enzyme-linked immunosorbent assay kit. Triglyceride (TG), total cholesterol (TC), low-density lipoprotein cholesterol (LDL-C) and high-density lipoprotein cholesterol (HDL-C) concentrations were measured using enzymatic colorimetric methods. Plasma concentrations of apolipoprotein A-I (apoA-I) was determined with an ELISA kit. For fast protein liquid chromatography (FPLC) analysis, 100 μ l pooled plasma was separated on a Superose 6 column (Amersham) at a flow rate of 0.5 ml/min as described previously⁴⁶. Hepatic lipid contents were measured by a spectrophotometric procedure as described⁴⁷.

Statistical Analysis. Data were presented as means \pm SE. Comparisons among groups were made using ANOVA, followed by a post hoc (PLSD) test to compare two individual groups. Differences were considered statistically significant at $P < 0.05$.

References

- Samal, B. *et al.* Cloning and characterization of the cDNA encoding a novel human pre-B-cell colony-enhancing factor. *Mol Cell Biol.* **14**, 1431–1437 (1994).
- Fukuhara, A. *et al.* Visfatin: a protein secreted by visceral fat that mimics the effects of insulin. *Science.* **307**, 426–430 (2005).
- Sun, Q. *et al.* Overexpression of visfatin/PBEF/Nampt alters whole-body insulin sensitivity and lipid profile in rats. *Ann Med.* **41**, 311–320 (2009).
- Revollo, J. R., Grimm, A. A. & Imai, S. The NAD biosynthesis pathway mediated by nicotinamide phosphoribosyltransferase regulates Sir2 activity in mammalian cells. *J. Biol Chem.* **279**, 50754–50763 (2004).
- Revollo, J. R. *et al.* Nampt/PBEF/Visfatin regulates insulin secretion in beta cells as a systemic NAD biosynthetic enzyme. *Cell Metab.* **6**, 363–375 (2007).
- Garten, A., Petzold, S., Korner, A., Imai, S. & Kiess, W. Nampt: linking NAD biology, metabolism and cancer. *Trends Endocrinol Metab.* **20**, 130–138 (2009).
- Berndt, J. *et al.* Plasma visfatin concentrations and fat depot-specific mRNA expression in humans. *Diabetes.* **54**, 2911–2916 (2005).
- Haider, D. G. *et al.* Increased plasma visfatin concentrations in morbidly obese subjects are reduced after gastric banding. *J. Clin Endocrinol Metab.* **91**, 1578–1581 (2006).
- Ingelsson, E. *et al.* Clinical correlates of circulating visfatin levels in a community-based sample. *Diabetes Care.* **30**, 1278–1280 (2007).
- Kiess, W. *et al.* Adipocytes and adipose tissue. *Best Pract Res Clin Endocrinol Metab.* **22**, 135–153 (2008).

11. Retnakaran, R. *et al.* Correlation of circulating full-length visfatin (PBEF/NAMPT) with metabolic parameters in subjects with and without diabetes: a cross-sectional study. *Clin Endocrinol (Oxf)*. **69**, 885–893 (2008).
12. Moschen, A. R. *et al.* Visfatin, an adipocytokine with proinflammatory and immunomodulating properties. *J Immunol*. **178**, 1748–1758 (2007).
13. Kang, J., Cheng, B. & Jiang, L. PPARgamma signal transduction pathway in the foam cell formation induced by visfatin. *Sheng Li Xue Bao*. **62**, 427–432 (2010).
14. Zhou, F. *et al.* Visfatin induces cholesterol accumulation in macrophages through up-regulation of scavenger receptor-A and CD36. *Cell Stress Chaperones*. **18**, 643–652 (2013).
15. Chinetti, G. *et al.* PPAR-alpha and PPAR-gamma activators induce cholesterol removal from human macrophage foam cells through stimulation of the ABCA1 pathway. *Nat Med*. **7**, 53–58 (2001).
16. Taniguchi, C. M., Ueki, K. & Kahn, R. Complementary roles of IRS-1 and IRS-2 in the hepatic regulation of metabolism. *J Clin Invest*. **115**, 718–727 (2005).
17. Brunetti-Pierri, N. *et al.* Acute toxicity after high-dose systemic injection of helper-dependent adenoviral vectors into nonhuman primates. *Hum Gene Ther*. **15**, 35–46 (2004).
18. Bristol, J. A., Shirley, P., Idamakanti, N., Kaleko, M. & Connelly, S. *In vivo* dose threshold effect of adenovirus-mediated factor VIII gene therapy in hemophilic mice. *Mol Ther*. **2**, 223–232 (2000).
19. Zhang, L. *et al.* GLP-1 analogue prevents NAFLD in ApoE mice with diet and Acpr30 knockdown by inhibiting c-JNK. *Liver Int*. **33**, 794–804 (2013).
20. Wang, C. *et al.* Silencing of FGF-21 expression promotes hepatic gluconeogenesis and glycogenolysis by regulation of the STAT3-SOCS3 signal. *FEBS J*. **281**, 2136–2147 (2014).
21. Salagianni, M. *et al.* Toll-like receptor 7 protects from atherosclerosis by constraining “inflammatory” macrophage activation. *Circulation*. **126**, 952–962 (2012).
22. Dahl, T. *et al.* Nicotinamide phosphoribosyltransferase and lipid accumulation in macrophages. *Eur J Clin Invest*. **41**, 1098–1104 (2011).
23. Li, Y. *et al.* Extracellular Nampt promotes macrophage survival via a nonenzymatic interleukin-6/STAT3 signaling mechanism. *J Biol Chem*. **283**, 34833–34843 (2008).
24. Rader, D. J., Alexander, E. T., Weibel, G. L., Billheimer, J. & Rothblat, G. H. The role of reverse cholesterol transport in animals and humans and relationship to atherosclerosis. *J Lipid Res*. **50**, Suppl, S189–194 (2009).
25. Nakaya, K. *et al.* Peroxisome proliferator-activated receptor-alpha activation promotes macrophage reverse cholesterol transport through a liver X receptor-dependent pathway. *Arterioscler Thromb Vasc Biol*. **31**, 1276–1282 (2011).
26. Rotllan, N. *et al.* Differential effects of gemfibrozil and fenofibrate on reverse cholesterol transport from macrophages to feces *in vivo*. *Biochim Biophys Acta*. **1811**, 104–110 (2011).
27. Jawien, J. *et al.* Inhibition of five lipoxygenase activating protein (FLAP) by MK-886 decreases atherosclerosis in apoE/LDLR-double knockout mice. *Eur J Clin Invest*. **36**, 141–146 (2006).
28. Uz, T., Dimitrijevic, N., Imbesi, M., Manev, H. & Manev, R. Effects of MK-886, a 5-lipoxygenase activating protein (FLAP) inhibitor, and 5-lipoxygenase deficiency on the forced swimming behavior of mice. *Neurosci Lett*. **436**, 269–272 (2008).
29. Huang, T. H. *et al.* Gypenoside XLIX isolated from *Gynostemma pentaphyllum* inhibits nuclear factor- kappaB activation via a PPAR-alpha-dependent pathway. *J Biomed Sci*. **13**, 535–548 (2006).
30. Yun, M. R. *et al.* Cilostazol Attenuates 4- hydroxynonenal- enhanced CD36 Expression on Murine Macrophages via Inhibition of NADPH Oxidase- derived Reactive Oxygen Species Production. *Korean J Physiol Pharmacol*. **13**, 99–106 (2009).
31. Huang, X. S. *et al.* Atorvastatin and fenofibrate increase apolipoprotein AV and decrease triglycerides by up-regulating peroxisome proliferator-activated receptor-alpha. *Br J Pharmacol*. **158**, 706–712 (2009).
32. Kehrer, J. P. *et al.* Inhibition of peroxisome-proliferator-activated receptor (PPAR) alpha by MK886. *Biochem J*. **356**, 899–906 (2001).
33. Tang, W. X. *et al.* Peroxisome proliferator-activated receptor- α activation protects against endoplasmic reticulum stress-induced HepG2 cell apoptosis. *Mol Cell Biochem*. **385**, 179–90 (2014).
34. Mulay, V. *et al.* Inhibition of mitogen-activated protein kinase Erk1/2 promotes protein degradation of ATP binding cassette transporters A1 and G1 in CHO and HuH7 cells. *PLoS One*. **25**, e62667 (2013).
35. Nencioni, A. *et al.* Nicotinamide phosphoribosyltransferase inhibition reduces intraplaque CXCL1 production and associated neutrophil infiltration in atherosclerotic mice. *Thromb Haemost*. **111**, 308–322 (2014).
36. Li, L. *et al.* The adipose triglyceride lipase, adiponectin and visfatin are downregulated by tumor necrosis factor-alpha (TNF-alpha) *in vivo*. *Cytokine*. **45**, 12–19 (2009).
37. Li, L. *et al.* Liraglutide prevents hypo adiponectinemia-induced insulin resistance and alterations of gene expression involved in glucose and lipid metabolism. *Mol Med*. **17**, 1168–1178 (2011).
38. Moore, K. J. *et al.* Loss of receptor-mediated lipid uptake via scavenger receptor A or CD36 pathways does not ameliorate atherosclerosis in hyperlipidemic mice. *J Clin Invest*. **115**, 2192–2201 (2005).
39. Cole, J. E. *et al.* Unexpected protective role for Toll- like receptor 3 in the arterial wall. *Proc Natl Acad Sci USA*. **108**, 2372–2377 (2011).
40. Bursill, C. A., Choudhury, R. P., Ali, Z., Greaves, D. R. & Channon, K. M. Broad- spectrum CC-chemokine blockade by gene transfer inhibits macrophage recruitment and atherosclerotic plaque formation in apolipoprotein E-knockout mice. *Circulation*. **110**, 2460–2466 (2004).
41. Tran-Lundmark, K. *et al.* Heparan sulfate in perlecan promotes mouse atherosclerosis: roles in lipid permeability, lipid retention, and smooth muscle cell proliferation. *Circ Res*. **103**, 43–52 (2008).
42. Zhang, Y. *et al.* Overexpression of apolipoprotein A-I promotes reverse transport of cholesterol from macrophages to feces *in vivo*. *Circulation*. **108**, 661–663 (2003).
43. Zhang, Y. *et al.* Hepatic expression of scavenger receptor class B type I (SR-BI) is a positive regulator of macrophage reverse cholesterol transport *in vivo*. *J Clin Invest*. **115**, 2870–2874 (2005).
44. Naik, S. U. *et al.* Pharmacological activation of liver X receptors promotes reverse cholesterol transport *in vivo*. *Circulation*. **113**, 90–97 (2006).
45. Pires, E. S., Parte, P. P., Meherji, P. K., Khan, S. A. & Khole, V. V. Naturally occurring anti-albumin antibodies are responsible for false positivity in diagnosis of autoimmune premature ovarian failure. *J Histochem Cytochem*. **54**, 397–405 (2006).
46. Collins, L. A. & Olivier, M. Quantitative comparison of lipoprotein fractions derived from human plasma and serum by liquid chromatography-tandem mass spectrometry. *Proteome Sci*. **8**, 42 (2010).
47. Ramesha, C. S., Paul, R. & Ganguly, J. Effect of dietary unsaturated oils on the biosynthesis of cholesterol, and on biliary and fecal excretion of cholesterol and bile acids in rats. *J Nutr*. **110**, 2149–2158 (1980).

Acknowledgements

This work was supported by research grants from the National Natural Science Foundation of China (81501199).

Author Contributions

S.L. supplemented data and revised the manuscript. C.W., K.L., M.T., J.X. and M.Y. contributed to data collection. Y.J., J.H. and L.G. researched and analyzed the data. G.B. reviewed and edited the manuscript. L.L. and H.L. drafted the manuscript. G.Y. designed the study's analytic strategy. All authors reviewed the manuscript.

Additional Information

Supplementary information accompanies this paper at <http://www.nature.com/srep>

Competing financial interests: The authors declare no competing financial interests.

How to cite this article: Li, S. *et al.* NAMPT knockdown attenuates atherosclerosis and promotes reverse cholesterol transport in ApoE KO mice with high-fat-induced insulin resistance. *Sci. Rep.* **6**, 26746; doi: 10.1038/srep26746 (2016).



This work is licensed under a Creative Commons Attribution 4.0 International License. The images or other third party material in this article are included in the article's Creative Commons license, unless indicated otherwise in the credit line; if the material is not included under the Creative Commons license, users will need to obtain permission from the license holder to reproduce the material. To view a copy of this license, visit <http://creativecommons.org/licenses/by/4.0/>